



Geochemical and isotopic evidence on the recharge and circulation of geothermal water in the Tangshan Geothermal System near Nanjing, China: implications for sustainable development

Lianghua Lu^{1,2} · Zhonghe Pang^{1,2} · Yanlong Kong^{1,2} · Qi Guo^{1,3} · Yingchun Wang^{1,2} · Chenghua Xu^{4,5} · Wen Gu⁴ · Lingling Zhou⁴ · Dandan Yu⁴

Received: 12 July 2017 / Accepted: 31 December 2017 / Published online: 18 January 2018
© Springer-Verlag GmbH Germany, part of Springer Nature 2018

Abstract

Geothermal resources are practical and competitive clean-energy alternatives to fossil fuels, and study on the recharge sources of geothermal water supports its sustainable exploitation. In order to provide evidence on the recharge source of water and circulation dynamics of the Tangshan Geothermal System (TGS) near Nanjing (China), a comprehensive investigation was carried out using multiple chemical and isotopic tracers ($\delta^2\text{H}$, $\delta^{18}\text{O}$, $\delta^{34}\text{S}$, $^{87}\text{Sr}/^{86}\text{Sr}$, $\delta^{13}\text{C}$, ^{14}C and ^3H). The results confirm that a local (rather than regional) recharge source feeds the system from the exposed Cambrian and Ordovician carbonate rocks area on the upper part of Tangshan Mountain. The reservoir temperature up to 87 °C, obtained using empirical as well as theoretical chemical geothermometers, requires a groundwater circulation depth of around 2.5 km. The temperature of the geothermal water is lowered during upwelling as a consequence of mixing with shallow cold water up to a 63% dilution. The corrected ^{14}C age shows that the geothermal water travels at a very slow pace (millennial scale) and has a low circulation rate, allowing sufficient time for the water to become heated in the system. This study has provided key information on the genesis of TGS and the results are instructive to the effective management of the geothermal resources. Further confirmation and even prediction associated with the sustainability of the system could be achieved through continuous monitoring and modeling of the responses of the karstic geothermal reservoir to hot-water mining.

Keywords Geothermal field · Hydrochemistry · Isotopes · Groundwater recharge · China

Published in the special issue “Groundwater sustainability in fast-developing China”

Electronic supplementary material The online version of this article (<https://doi.org/10.1007/s10040-018-1721-6>) contains supplementary material, which is available to authorized users.

✉ Zhonghe Pang
z.pang@mail.iggcas.ac.cn

- ¹ Key Laboratory of Shale Gas and Geoengineering, Institute of Geology and Geophysics, Chinese Academy of Sciences, Beijing 100029, China
- ² University of Chinese Academy of Sciences, Beijing 100049, China
- ³ China Minmetals Corporation, Beijing 10010, China
- ⁴ The 1st Geological Brigade of Jiangsu Geology and Mineral Exploration Bureau, Nanjing 210041, China
- ⁵ School of Earth Sciences and Engineering, Hohai University, Nanjing 210098, China

Introduction

Geothermal resources, consisting of heat, minerals and water, are one of the most practical and competitive clean-energy sources available as a viable alternative to fossil fuels to mitigate global climate change (Kong et al. 2014; Michael et al. 2010; Wang 2009; Wang et al. 2015). The global development of geothermal energy has become more and more rapid since the 1970s (Lund and Boyd 2016) because it is widely distributed, environmentally friendly and economically profitable (Montanari et al. 2017; Yang et al. 2017); however, uncontrolled mining of geothermal water may result in continuous decline of the water table and the reservoir temperature (Duan et al. 2011), which is not sustainable. Sustainable use of geothermal resources is a new challenge for the scientific community (Hähnlein et al. 2013; Mongillo 2010).

Systematic hydrochemical and isotopic studies on geothermal systems are essential tools toward effective exploration

and sustainable use of geothermal resources (Guo et al. 2010; Kong et al. 2014; Reinsch et al. 2013). Different aspects of a geothermal/groundwater system can be unveiled with different hydrogeochemical and isotopic methods. Stable $\delta^{18}\text{O}$ and $\delta^2\text{H}$ isotopes combined with hydrochemistry have been widely used in tracing sources of groundwater and delineating water–rock–gas interaction processes occurring in groundwater systems (Awaleh et al. 2015; Bo et al. 2015; Bozdağ 2016; Chandrajith et al. 2013; Diamond and Harris 2000; Ghomshei and Clark 1993; Guo et al. 2010; Li et al. 2017; Ma et al. 2009; Majumdar et al. 2005; Pang 2011; Wang et al. 2016; Xu et al. 2017). In the past two decades, the Sr isotopic ratio of $^{87}\text{Sr}/^{86}\text{Sr}$ has been widely used as a tracer for delineating hydrogeochemical processes, the origin of groundwater and chemical components, and the mixing effect in groundwater systems (Bakari et al. 2013; Barbieri and Morotti 2003; Boschetti et al. 2005; Brenot et al. 2015; Grobe et al. 2000; Guo et al. 2010; Khaska et al. 2015; Wang et al. 2006). The sulfur isotope $\delta^{34}\text{S}$ in sulfate has been commonly used to trace the origin of sulfate content, groundwater evolution and water–rock interactions occurring in groundwater systems (Al-Charideh 2015; Raidla et al. 2014; Sack and Shama 2014). Groundwater age can be used to evaluate the circulation rate and renewability of groundwater (Huang et al. 2017a, b) and ^{14}C in dissolved inorganic carbon (DIC) has been commonly used for age determination by hydrogeologists (Edmunds et al. 2006; Han et al. 2014; Huang et al. 2017b). While empirical chemical geothermometers including quartz (Fournier 1977), chalcedony (Fournier, 1977), and cation geothermometers (Fournier 1979; Fournier and Truesdel 1973; Fournier and Potter 1979; Giggenbach 1988; Pang et al. 2013) are still used to predict reservoir temperature, it is now quite common that theoretical chemical geothermometers based on a chemical thermodynamic modeling approach are used, which was proposed and improved by Reed and Spycher (1984), Pang and Reed (1998) and Spycher et al. (2013).

In China, geothermal resources are widely distributed, especially the low-medium temperature hydrothermal resources (Lund and Boyd 2016; Wang et al. 1993). Low-medium temperature geothermal systems hosted in carbonate rocks are some of the most promising and unknown geothermal systems (Kong et al. 2015; Montanari et al. 2017; Pang et al. 2015). Tangshan area is one of the most famous “hot spring towns” in China (Zhao and Zhu 1998) with a low-medium temperature convective geothermal system developed in carbonate rocks. With the rapid development of tourism, the demand for geothermal resources has increased significantly (Zhao and Zhu 1998). During the past two decades, rapid decline of the water level has occurred in many geothermal wells, with all historical hot springs having vanished and some geothermal wells dried up (Zhao and Zhu 1998). In order to achieve sustainable use of geothermal water in Tangshan, it is necessary to fill the

knowledge gap on Tangshan Geothermal System (TGS); however, to the best knowledge of the authors, limited hydrogeochemical and isotopic studies on TGS have been carried out. The previous studies have revealed the geological background and tectonic framework of the system. They speculated on the genesis of TGS based on geological information (Li et al. 2010; Luan and Qiu 1998; Zhao and Zhu 1998) with limited analyses on hydrochemistry and stable isotopes ($\delta^2\text{H}$ and $\delta^{18}\text{O}$; Zou et al. 2015).

In order to achieve a comprehensive understanding on TGS, a multi-tracer approach involving hydrochemistry and isotopes ($\delta^2\text{H}$, $\delta^{18}\text{O}$, $\delta^{34}\text{S}$, $^{87}\text{Sr}/^{86}\text{Sr}$, $\delta^{13}\text{C}$, ^{14}C , ^3H) was implemented, aiming at solving a few key scientific issues: (1) Does the geothermal system get water recharge from a local source or a remote source? (2) What is the groundwater circulation rate and what are the implications of that on the sustainable use of geothermal water?

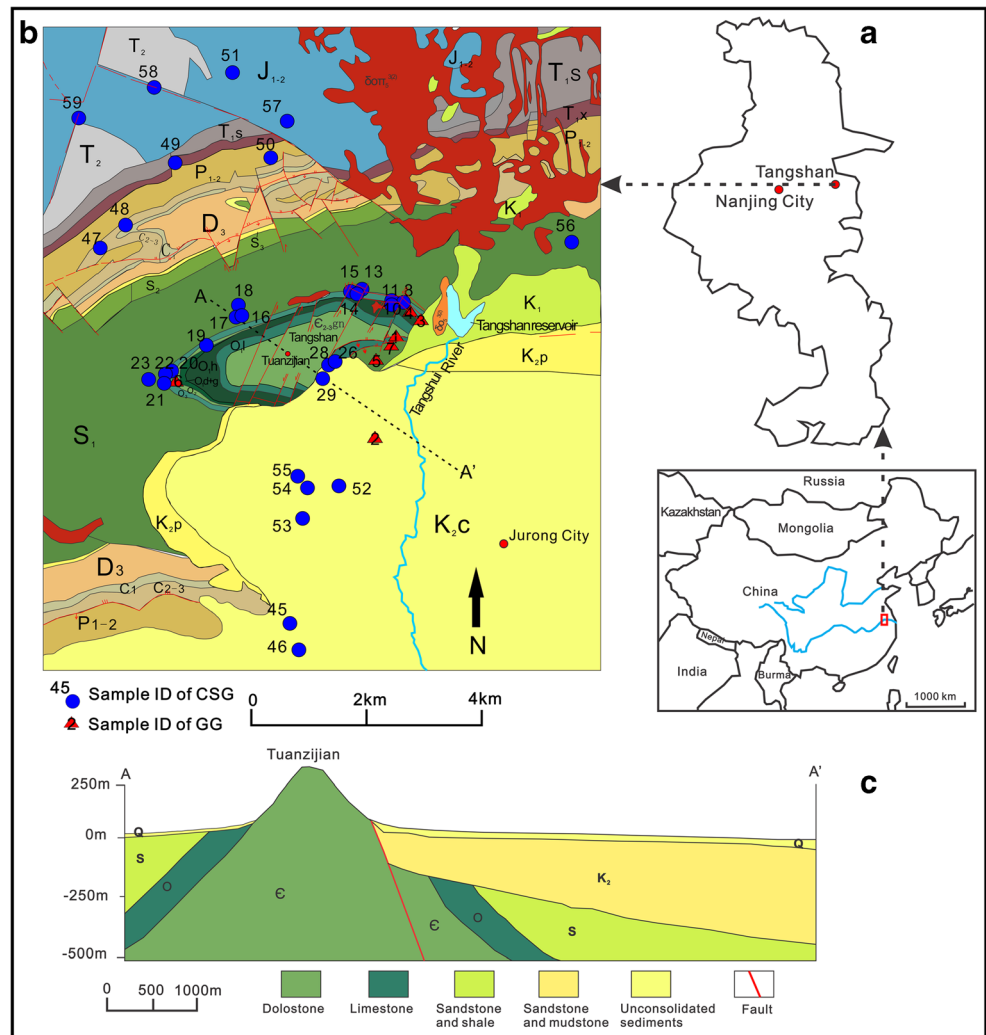
Study area

TGS is located in the eastern suburb of city of Nanjing, Jiangsu Province, which is approximately 25 km (Fig. 1a) from the downtown of Nanjing. Tangshan area features a subtropical monsoon climate with an annual average temperature of 15.4 °C and annual average precipitation of 1,060 mm. The main surface-water system here is Tangshui River and Tangshan reservoir to the east of Tangshan (Fig. 1b). Tangshan Mountain is approximately east–west trending, and about 5 km long and 3 km wide. The main geomorphologies are low mountains and hills with elevation varying from 150 to 300 m a.s.l, and the peak is Tuanzujian Mountain (Fig. 1b) with an elevation of about 300 m a.s.l. in the middle of Tangshan (Zou et al. 2015).

Sedimentary strata developed in the region are almost continuous from Cambrian to Cretaceous periods; however, the main strata developed in Tangshan are dolomite of the Cambrian system, limestone of the Ordovician system, sandstone and shale of the Silurian system, and sandstone and mudstone of the Cretaceous system, with Devonian to Jurassic systems missing (Zhao and Zhu 1998). The Cambrian and Ordovician systems are exposed over Tangshan and form the Tangshan body. The Silurian system is mainly represented in the west and north of Tangshan, while the Cretaceous system is mainly distributed in the east and south of Tangshan (Fig. 1b). Quaternary formations are widely distributed in the piedmont area and valley with thickness varying from 2 to 40 m. Quartz diorite porphyry of Yanshan age is mainly presented in the north of Tangshan (Zou et al. 2015).

Tectonically, Tangshan is located in the west part of Ningzhen uplift structure bordered by Tangshan-Dongchangjie fault to the south of Tangshan (Luan and Qiu

Fig. 1 **a** Location of the town Tangshan in China; **b** Geological map and sampling sites at and around Tangshan (different strata are indicated with different colors and corresponding symbols); **c** Geological cross section of study area



1998). Locally, Tangshan is located in the center of the Tangshan-Lunshan anticlinorium. The core of the Tangshan anticline is made of Cambrian and Ordovician systems, while the flanks are composed of the Silurian system. Three groups of fault structures, NE, NW and EW faults, developed in Tangshan, which are mainly distributed in the east, middle and south of Tangshan. The east part of Tangshan anticline was cut by NW and NE faults, resulting in the falling of formations in the east (Fig. 1c).

The aquifers developed here can be classified into two categories: porous formation in unconsolidated Quaternary sediments, and fractured bedrock (karstic and clastic rocks). The Quaternary formations are low in permeability. Karstic groundwater, including cold and thermal groundwaters, is distributed in the carbonate rock formations of Cambrian and Ordovician systems with high permeability. The cold karstic groundwater is mainly present in the middle of Tangshan Mountain, while thermal karstic groundwater is in the east and west of Tangshan. Fractured aquifers in clastic rocks mainly appear in the sandstone and shale of the Silurian and

Cretaceous systems, in which fractures are less developed and permeability is much lower, and can be regarded as aquitards. The water table in Tangshan has significantly declined (up to 10 m) during recent years due to increased use of geothermal resources. In this study, thermal water samples were collected from Cambrian and Ordovician aquifers and cold shallow samples mainly from Quaternary, Silurian and Cretaceous aquifers with three from carbonate rock aquifers.

Tangshan Geothermal System (TGS) is a low-medium temperature convective geothermal system (Luan and Qiu 1998; Wang et al. 1993). The regional terrestrial heat flow is 54–58 mW/m², and the average geothermal gradient is 26–28 °C/km in the depth range of a few hundred meters. The wellhead temperature is about 50–65 °C in the eastern and 30–39 °C in the western ends of the mountain. The geothermal reservoirs are composed of carbonate rocks of Cambrian and Ordovician systems. The caprock, mainly distributed in the piedmont area of Tangshan, mainly consisted of formations of Quaternary, Silurian and Cretaceous systems (Li et al. 2010; Zhao and Zhu 1998). The locally developed faults and

other structures provide good circulation channels for geothermal water.

Materials and methods

Collection of samples

A sampling campaign was implemented in April 2016, in which a total of 46 water samples were collected including 2 samples from Tangshui River, 5 samples from Tangshan reservoir, 32 samples from drinking water wells and 7 samples from geothermal wells. The groundwater sampling locations are shown in Fig. 1b. All samples for hydrochemical analyses were filtered with a 0.45- μm membrane before bottling. Samples for cation and trace elements analysis were acidified with ultra-purified HNO_3 to adjust the sample to $\text{pH} < 2$. Filtered 60 ml of water were collected into HDPE vials for anion analyses. A total of 20 ml of filtered water was collected into screw capped HDPE vials for stable $\delta^{18}\text{O}$ and $\delta^2\text{H}$ analyses, whereas 1,000 ml of unfiltered water was collected into screw capped HDPE bottles for $\delta^{13}\text{C}$ and ^{14}C analyses, 200 ml of water for $^{87}\text{Sr}/^{86}\text{Sr}$ analyses, and 1,000 ml of water for $\delta^{34}\text{S}$ analyses.

Analytical methods

Physical and chemical parameters such as pH, total dissolved solids (TDS), temperature, electrical conductivity, and redox potential (Eh), were measured on site using a multi-parameter device, the Hach HQ40D. HCO_3^- was analyzed on site by a digital titrator (Model 16900, Hach) with 0.8 N H_2SO_4 using bromocresol green-methyl red indicator. Other chemical and isotopic analyses were performed in laboratories within about 1 week after collection. The main anions (F, Cl, and SO_4 , with detection limit of 0.1 mg/L) and cations were determined using a Dionex-500 ion chromatograph (detection limit is 0.1 mg/L) in the Water Isotope and Water–Rock Interaction Laboratory at the Institute of Geology and Geophysics, Chinese Academy of Sciences (IGG-CAS). Trace elements (Sr, Si, etc.) were measured by ICP-MS (detection limit is 0.1 $\mu\text{g}/\text{L}$) in the Analytical Laboratory of the Beijing Research Institute of Uranium Geology (BRIUG). Stable isotopes ($\delta^{18}\text{O}$, $\delta^2\text{H}$) were analyzed in the Water Isotope and Water–Rock Interaction Laboratory at IGG-CAS by the laser absorption water isotope analyzer Picarro L1102-i (the precision of the $\delta^{18}\text{O}$ and $\delta^2\text{H}$ values were ± 0.1 and $\pm 0.5\%$, respectively). $\delta^{13}\text{C}$ and ^{14}C in groundwater samples were measured at Beta Analytic in the USA using accelerator mass spectrometry (AMS). The analytical precision was $\pm 0.1\%$ for $\delta^{13}\text{C}$ and ± 0.1 pmC for ^{14}C . $^{87}\text{Sr}/^{86}\text{Sr}$ of groundwater samples was measured in the Analytical Laboratory of BRIUG by Phoenix TIMS stable isotope mass spectrometry.

The $\delta^{34}\text{S}$ in dissolved SO_4^{2-} was measured in the stable isotopes laboratory of IGG-CAS by MAT 253 stable isotope mass spectrometry. The results of water chemistry and isotopic compositions of water samples are shown in Table S1 of the electronic supplementary material (ESM). The software PHQEERC 3.0 and the lnl.dat dataset (Parkhurst and Appelo 2013) developed by the United States Geological Survey (USGS) was applied to calculate the mineral saturation index (SI).

Results

Water chemistry

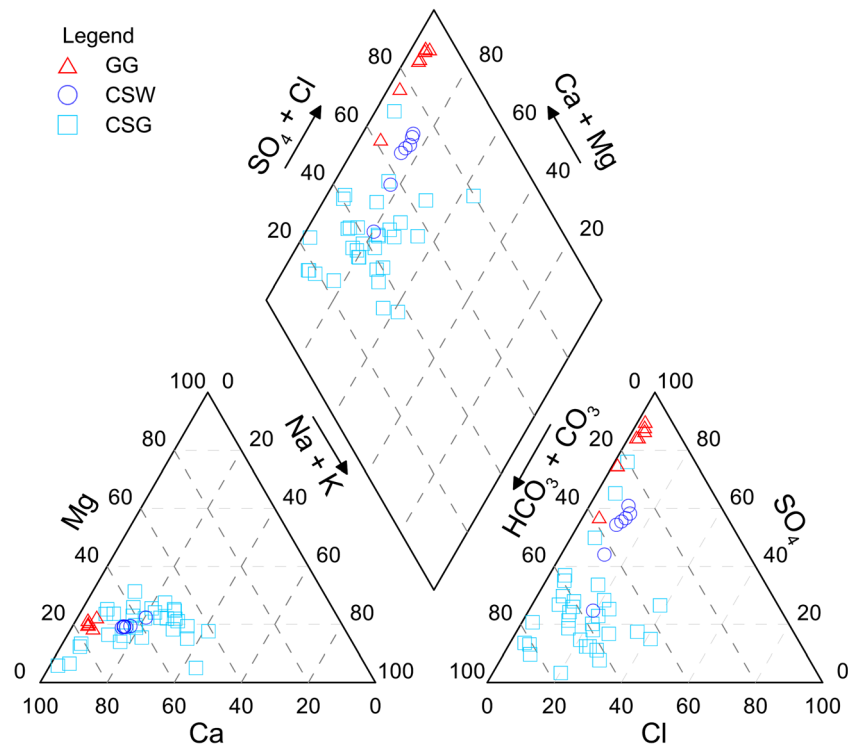
The results of water chemistry analyses are given in Table S1 of the ESM. Based on the properties and chemical composition, the water samples can be divided into three categories: cold surface water (CSW) (including reservoir and river water), cold shallow groundwater (CSG), and geothermal groundwater (GG). The charge balances of all samples are within $\pm 5\%$ (Table S1 of the ESM).

A Piper plot of all water samples is shown in Fig. 2. For CSW, the pH varies from 8.6 to 9.0. The dominant anions are SO_4 and HCO_3^- with SO_4 ranging from 60.1 to 154.7 mg/L and HCO_3^- from 84.4 to 173.3 mg/L. The dominant cation is Ca with a concentration range of 62.5 to 80.0 mg/L. The water type is mainly HCO_3^- -Ca/ SO_4 - HCO_3^- -Ca (Fig. 2; Table S1 of the ESM) with TDS ranging from 291.0 to 352.0 mg/L (Table S1 of the ESM).

The CSG samples were mainly taken from Quaternary, Silurian and Cretaceous aquifers. The pH varies from 6.9 to 10.8. The dominant cation and anion are Ca and HCO_3^- with the concentration range of 52.1–151.1 mg/L and 7.3–389.0 mg/L for Ca and HCO_3^- , respectively. The water type is mainly HCO_3^- -Ca/ HCO_3^- - SO_4 -Ca (Fig. 2; Table S1 of the ESM) with TDS ranging from 193.0 to 819.0 mg/L (Table S1 of the ESM). The concentration range of Sr is from 143.0 to 846.0 mg/L.

The GG samples were mainly taken from Ordovician and Cambrian carbonate aquifers. The pH varies from 7.1 to 8.0. The concentrations of Sr and SO_4 are the highest in GG samples, with the content range of 6,921.0 to 10,488.0 $\mu\text{g}/\text{L}$ and 319.8 to 1,012.9 mg/L for Sr and SO_4 , respectively, compared to CSW and CSG samples. The dominant cation is Ca with concentration varying from 185.2 to 380.4 mg/L. The main water type is SO_4 -Ca (Fig. 2; Table S1 of the ESM) except sample 16D04 (SO_4 - HCO_3^- -Ca, which may be affected by mixing with CSG) with TDS ranging from 713.0 to 1,580.0 mg/L (Table S1 of the ESM). The wellhead temperatures measured on site vary from 34.1 to 65.3 $^\circ\text{C}$.

Fig. 2 Piper plot of all water samples (GG geothermal groundwater; CSW cold surface water; CSG cold shallow groundwater)



Isotopic compositions

The isotopic results are shown in Table S1 of the [ESM](#), which indicates that $\delta^2\text{H}$ and $\delta^{18}\text{O}$ in CSW are the most enriched, with $\delta^2\text{H}$ ranging from -24.8 to -34.5 ‰ and $\delta^{18}\text{O}$ from -3.8 to -5.1 ‰, followed by CSG with $\delta^2\text{H}$ ranging from -18.6 to -49.1 ‰ and $\delta^{18}\text{O}$ from -3.9 to -7.7 ‰ (Fig. 3). $\delta^2\text{H}$ and $\delta^{18}\text{O}$ in GG samples are the most depleted with $\delta^2\text{H}$ ranging from -49.1 to -55.8 ‰ and $\delta^{18}\text{O}$ from -7.5 to -8.6 ‰ (Fig. 3), which is probably related to higher recharge elevation.

$^{87}\text{Sr}/^{86}\text{Sr}$ analyses of seven GG samples and 17 CSG samples were conducted in this study (Table S1 of the [ESM](#)). The value of $^{87}\text{Sr}/^{86}\text{Sr}$ in GG samples is low with a narrow range of 0.709136 to 0.709210, while the value in CSG samples is relatively high with a wide range of 0.709514 to 0.713183 (Fig. 4a), which indicates different water–rock reactions between them.

$\delta^{34}\text{S}$ analyses of seven GG samples and 11 CSG samples were conducted in this study (Table S1 of the [ESM](#)). The $\delta^{34}\text{S}$ in GG samples is enriched, varying from 28.165 to 33.695 ‰, while that in CSG samples is relatively depleted with a range of 1.165 to 22.321 ‰ (Fig. 5). Meanwhile, the $\delta^{34}\text{S}$ value of most GG samples (85.7%) is around 30 ‰, while that of most (81.8%) CSG samples is below 10 ‰ (Fig. 5). $\delta^{34}\text{S}$ is controlled by different SO_4 sources.

A total of seven ^{14}C , $\delta^{13}\text{C}$, and tritium (^3H) samples of GG were measured (Table S1 of the [ESM](#)). The ^{14}C activities in dissolved inorganic carbon (DIC) of GG samples are

relatively low with values varying from 21.4 to 76.9 pmC (Fig. 6). The $\delta^{13}\text{C}$ in DIC of GG samples is relatively enriched with values varying from -13.2 to -9.1 ‰ (Fig. 6). ^3H was not detected in GG samples (therefore not shown in Table S1 of the [ESM](#)).

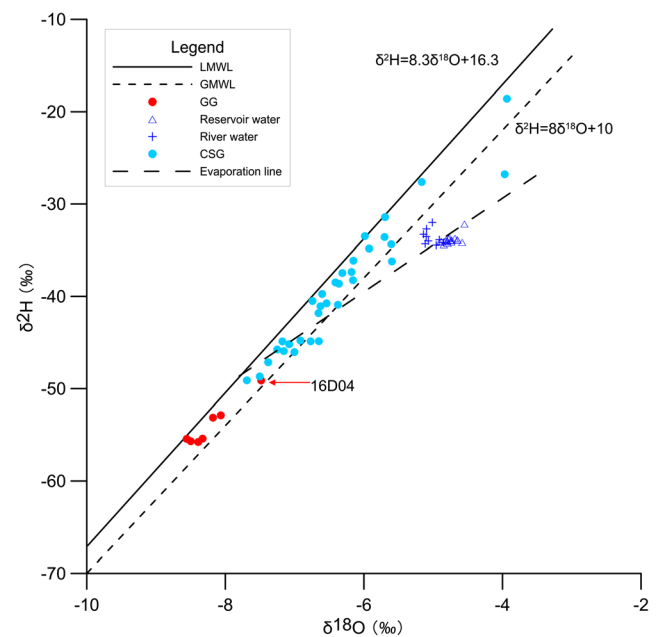


Fig. 3 The $\delta^2\text{H}$ - $\delta^{18}\text{O}$ relation plot of all water samples (some isotopic data of surface reservoir water are not presented in Table S1 of the [ESM](#); GG geothermal groundwater, CSG cold shallow groundwater)

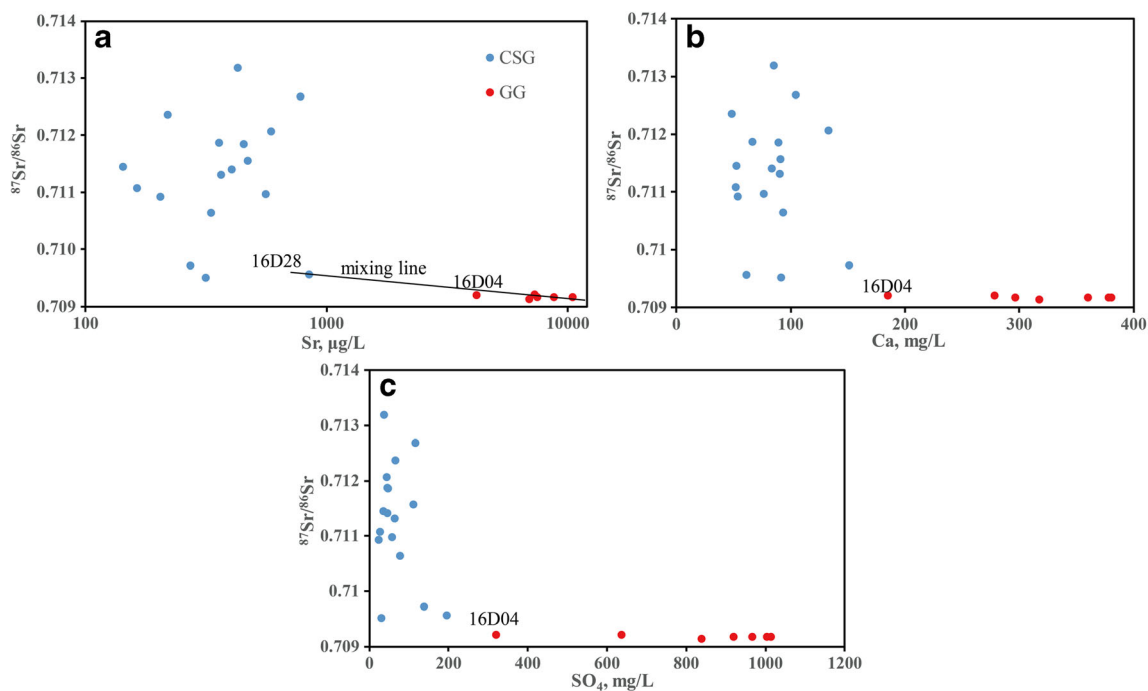


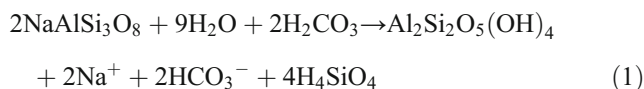
Fig. 4 The relation between $^{87}\text{Sr}/^{86}\text{Sr}$ and **a** Sr, **b** Ca, and **c** SO_4 for geothermal groundwater (GG) and cold shallow groundwater (CSG) samples

Discussion

Water–rock reactions

Water–rock reactions are important geochemical processes in geothermal water and shape the characteristics of water chemistry. The linear relationship between mNa and mCl (as mmol/L) is shown in Fig. 7a. All the GG samples plot near the line of mNa:mCl = 1:1, suggesting that Na and Cl were mainly derived from NaCl dissolution (Huang et al. 2017a); however, some CSG samples lie below the line of mNa:mCl = 1:1, indicating that apart from NaCl dissolution,

dissolution of albite in formations (Eq. 1) might contribute to the additional Na (Huang et al. 2017a):



The relationship between m(Ca + Mg) and mHCO₃ (as mmol/L) is given in Fig. 7b, between mCa and mMg is given in Fig. 7c, and mCa and mSO₄ is given in Fig. 7d (as meq/L). All GG samples lie above the line of m(Ca + Mg):mHCO₃ = 1:1, while the CSG samples plot on or below the line (Fig. 7b).

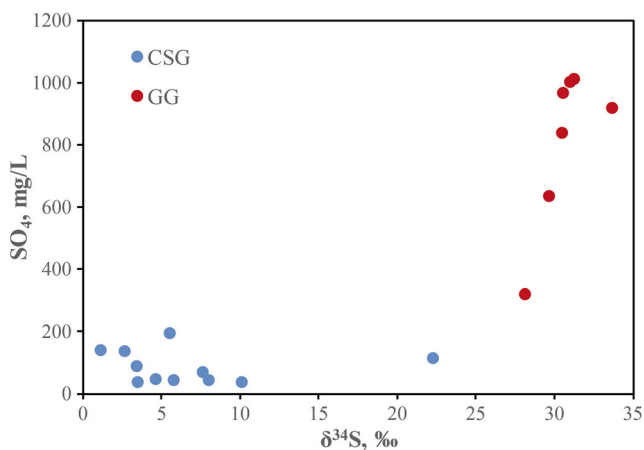


Fig. 5 The relation between $\delta^{34}\text{S}$ and SO_4 for geothermal groundwater (GG) and cold shallow groundwater (CSG) samples

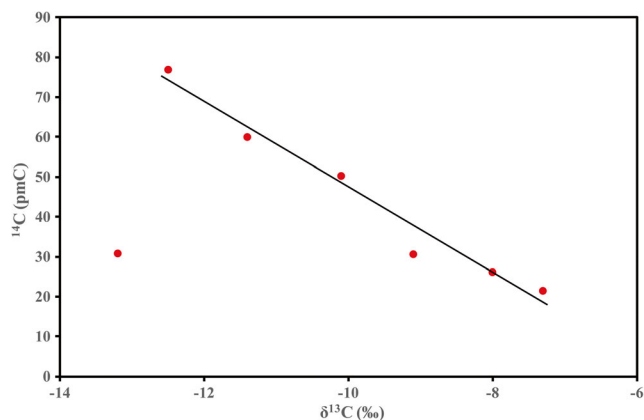
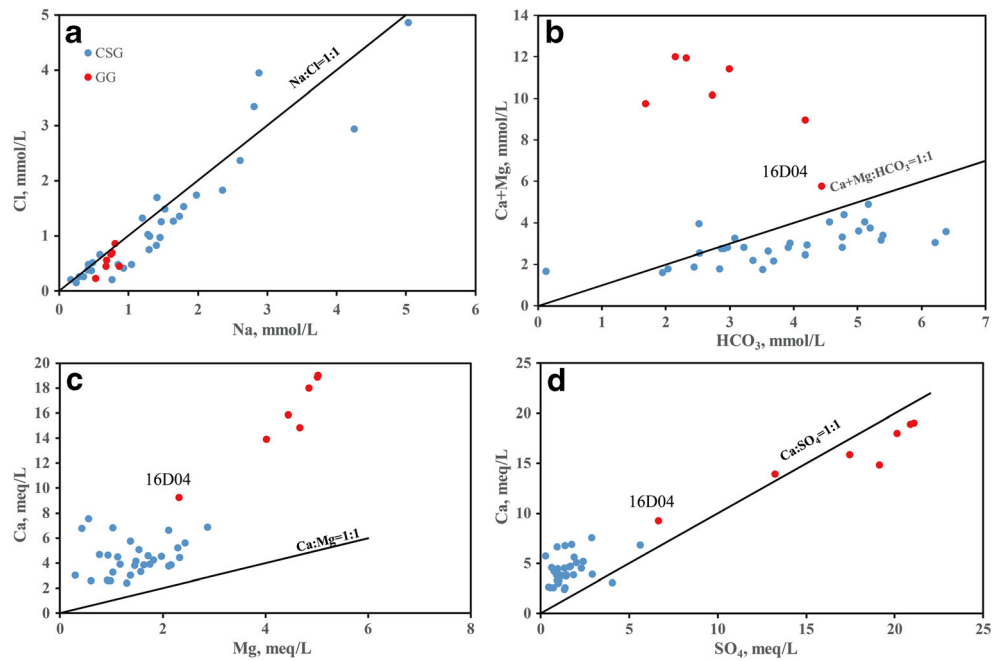


Fig. 6 The relation plot of ^{14}C - $\delta^{13}\text{C}$ for geothermal groundwater (GG) samples

Fig. 7 Major ion ratio relation **a** Na-Cl; **b** Ca + Mg-HCO₃; **c** Ca-Mg; **d** Ca-SO₄ of geothermal groundwater (GG) and cold shallow groundwater (CSG) samples



Although both of GG and CSG samples lie above the line of mCa:mMg = 1:1, the ratios of mCa to mMg are much greater in GG samples (Fig. 7c). All GG samples plot near or below the line of mCa:mSO₄ = 1:1, while most of CSG samples lie above the line (Fig. 7d). The different characteristics of chemical compositions suggest different water–rock interaction processes and weak connections between CSG and deep GG. If only dissolution of calcite and dolomite (Eqs. 3 and 4) occurred in the geothermal reservoir, the ratio of m(Ca + Mg) to mHCO₃ should be <1 (Huang et al. 2017a, b), which is not the case in this study. The high content of Ca and SO₄ and the ratio of mCa to mSO₄ close to 1 suggests that, except for carbonate dissolution, anhydrite (embedded in carbonate rock) dissolution (Eq. 2) also occurred (Ma et al. 2011) and it dominates the water–rock interaction processes in the geothermal reservoir, which is also demonstrated by mineral saturation indices (SI) and Sr and S isotopes (see the following discussion).

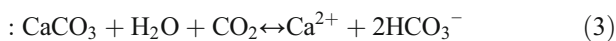
The mineral SI of GG samples are shown in Table 1. The SI of calcite and dolomite is greater than 0 and anhydrite (gypsum) is less than 0, suggesting precipitation tendency for carbonate minerals and dissolution tendency for gypsum, which is consistent with the hydrochemical results. The significant dissolution of gypsum may lead to precipitation of carbonate minerals to some extent, which consequently results in some GG samples lying below the line of mCa:mSO₄ = 1:1 (Fig. 7d; Ma et al. 2011). The significant negative values of SI of albite indicate that albite dissolution is probably much limited in the geothermal reservoir, which is in agreement with the hydrochemical results.

Dissolved Sr in groundwater is generally derived from geological components through water–rock interactions and cation exchange reactions (Bakari et al. 2013). The ⁸⁷Sr/⁸⁶Sr ratio is a good tracer of the rock type that has interacted with groundwater, and when combined with

Anhydrite dissolution/precipitation



Calcite dissolution/precipitation



Dolomite dissolution/precipitation

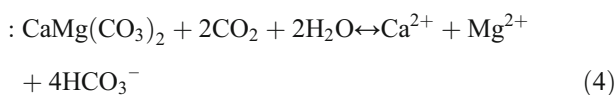


Table 1 Mineral saturation indices (SI) of geothermal groundwater (GG) samples

Sample ID	Calcite	Dolomite	Anhydrite	Gypsum	Albite
16D01	0.55	0.74	-0.42	-0.40	-3.93
16D02	0.99	1.67	-0.55	-0.40	-4.60
16D03	0.71	0.98	-0.19	-0.28	-4.07
16D04	0.96	1.52	-1.09	-0.89	-2.82
16D05	0.84	1.24	-0.18	-0.28	-4.05
16D06	0.56	0.76	-0.75	-0.54	-3.63
16D07	1.24	2.05	-0.21	-0.31	-4.03

chemical compositions it might be useful for identifying the potential water–rock interaction processes (Guo et al. 2010; Khaska et al. 2015; Wang et al. 2006). The $^{87}\text{Sr}/^{86}\text{Sr}$ ratios of GG samples are low (0.709136 ~ 0.709210, Fig. 4a) showing a typical carbonate or evaporite (gypsum, anhydrite) weathering source (Négré and Roy 1998), while those in CSG samples are relatively high (0.709514 ~ 0.713183) showing a typical silicate weathering source (Faure 1986; Négré and Roy 1998), which is consistent with the respective lithology of aquifers. The GG samples have low $^{87}\text{Sr}/^{86}\text{Sr}$ ratio and high Sr, Ca and SO_4 concentrations, while CSG samples have high $^{87}\text{Sr}/^{86}\text{Sr}$ ratio and low Sr, Ca and SO_4 concentrations (Fig. 4), indicating weak hydraulic connections between CSG and deep GG. Both Sr- SO_4 (Fig. 8a) and Sr-Ca (Fig. 8b) show a positive correlation. The $^{87}\text{Sr}/^{86}\text{Sr}$ ratio combined with hydrochemistry demonstrates that the high Sr content was mainly derived from carbonate and gypsum dissolution in GG. In other words, carbonate and gypsum dissolution are the main water–rock interaction processes.

The GG samples have high SO_4 content. $\delta^{34}\text{S}$ in dissolved SO_4 has been extensively used as a tracer for determining the source of SO_4 and the relevant geochemical processes (Raidla et al. 2014; Sack and Shama 2014). The GG samples are enriched in $\delta^{34}\text{S}$ (28.165 ~ 33.695 ‰), and the $\delta^{34}\text{S}$ values stay around 30 ‰ with increasing SO_4 concentration (Fig. 5), which suggests a typical sulfate (gypsum and anhydrite) dissolution source of SO_4 (Raidla et al. 2014). The GG samples have enriched $\delta^{34}\text{S}$ and high SO_4 concentration, while the CSG samples have relatively depleted $\delta^{34}\text{S}$ and low SO_4 concentration, demonstrating weak hydraulic connections between CSG and deep GG.

Reservoir temperature calculation

In case of no drilling temperature measurement, fluid geothermometry can be used to predict reservoir temperature. Cation geothermometry, theoretical chemical

geothermometry and silica (SiO_2) geothermometry were applied in this study to comprehensively evaluate the reservoir temperature.

Cation geothermometry

The results of cation geothermometry are shown in Table 2. The calculated temperatures are either too high for this study area or lower than wellhead temperature, which is not reasonable. The Giggenbach Na/1000-K/100-SQR (Mg) ternary plot (Giggenbach 1988) is a classic method to check the equilibrium state of geothermal water with relevant minerals and can also be used to predict reservoir temperature. The Giggenbach plot (not shown) shows that the GG samples lie in the immature water area, also indicating that cation geothermometry is unsuitable in this case.

SiO_2 geothermometry

This method is based on the dissolution equilibrium of SiO_2 in geothermal water to predict the reservoir temperature. The calculated results of different SiO_2 geothermometries are shown in Table 3. Only the chalcedony geothermometry gives a reasonable temperature and the calculated temperatures of 16D05 and 16D07 are close to that of theoretical chemical geothermometry. The calculated temperature of 16D04 is relatively low and probably is affected by mixing with CSG. The calculated temperatures of other methods are lower than the wellhead temperatures or even negative values, and therefore not suitable.

Theoretical chemical geothermometry

This method is used to verify whether the geothermal water in the reservoir has reached equilibrium with relevant mineral assemblages in the host rock (Pang and Reed 1998; Reed and Spycher 1984) and provides the reservoir temperature if equilibrium is established. The variations of the SI with increasing temperature were calculated using SOLVEQ-XPT

Fig. 8 The ion ratio relation of **a** Sr- SO_4 and **b** Sr-Ca for geothermal groundwater (GG) and cold shallow groundwater (CSG) samples

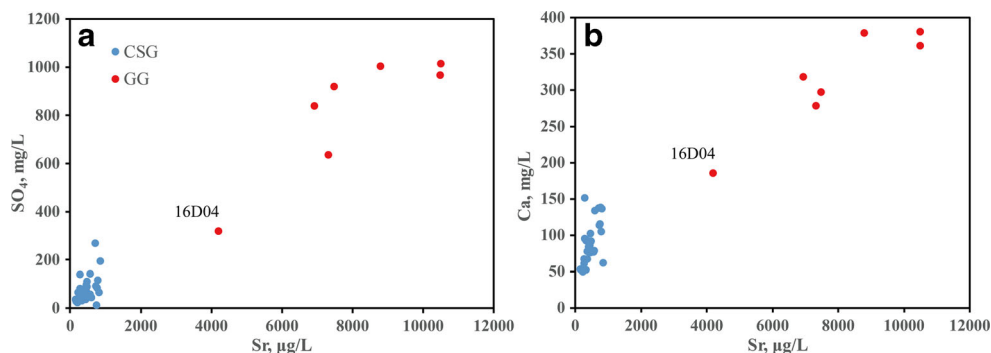


Table 2 Calculation results of cation geothermometry (in °C)

Sample ID	Wellhead Temp	Na-K-Ca ^a	Na/K ^b	Na/K ^c	Na/K ^d	Na/K ^e	Na/K ^f	K/Mg ^g
16D01	48.3	23	420	483	414	565	463	45
16D02	40.1	32	424	491	418	574	470	51
16D03	64.3	28	437	513	429	601	489	50
16D04	35.1	16	323	331	329	387	328	39
16D05	64.7	27	446	530	437	620	503	50
16D06	34.1	10	366	396	367	462	387	35
16D07	65.3	27	443	523	433	612	498	49

^a Fournier and Tressdell 1973^b Fournier 1979^c Truesdell 1976^d Giggenbach 1988^e Tonani 1980^f Arnorsson et al. 1983^g Giggenbach 1988

code (Reed et al. 2012). The two samples with the highest wellhead temperature, 16D05 and 16D07, were taken as examples of how to apply this method. The forced equilibrium of calcite was adopted to correct CO₂ degassing and the forced equilibrium of microcline was conducted to correct possible aluminum concentration error (Pang and Reed 1998). The possible mixing and dilution effects were also corrected (Pang and Reed 1998). The calculation results are shown in Fig. 9, which gives the temperature of 73–80 °C for 16D05 and 75–80 °C for 16D07.

From the preceding discussion, the calculated temperatures of chalcedony geothermometry are most reasonable and close to those of theoretical chemical geothermometry, and therefore regarded as the reservoir temperature in this study. The reservoir temperature in the west of Tangshan is about 51 °C (16D06), while that in the east of Tangshan is 74–87 °C, with an average of 80 °C and relatively high. The difference between the reservoir temperatures in the east and west of Tangshan is probably related to the depth of the geothermal reservoir, as the geothermal reservoir in the east is deeper due to the effect of the fault structure.

Table 3 Calculation results of different SiO₂ geothermometries (in °C)

Sample ID	Wellhead Temp	Amorphous silica ^a	α-cristobalite ^a	β-cristobalite ^b	Chalcedony ^a
16D01	48.3	−12	54	7	74
16D02	40.1	−43	18	−26	75
16D03	64.3	−5	62	14	83
16D04	35.1	−35	27	−18	45
16D05	64.7	−2	65	18	87
16D06	34.1	−30	33	−13	51
16D07	65.3	−6	61	14	82

^a Fournier 1977^b Fournier 1991

Groundwater circulation depth

The groundwater circulation depth can be calculated using the following equation (Li and Li 2010):

$$D = (T - T_0) / G \quad (5)$$

where D is circulation depth (km); T is reservoir temperature (°C); T_0 is the temperature of the constant temperature zone (°C); G is the geothermal gradient (°C/km). The groundwater circulation depth of 2.3–2.5 km was obtained with the average reservoir temperature of 80 °C assumed for T , annual average temperature of 15.4 °C for T_0 and average geothermal gradient of 26–28 °C/km for G .

Recharge source of geothermal water

H and O stable isotopes ($\delta^2\text{H}$ and $\delta^{18}\text{O}$) are good tracers for determining the recharge of groundwater as they carry the information of water itself. The relationship between $\delta^2\text{H}$ and $\delta^{18}\text{O}$ is shown in Fig. 3. The local meteoric water line

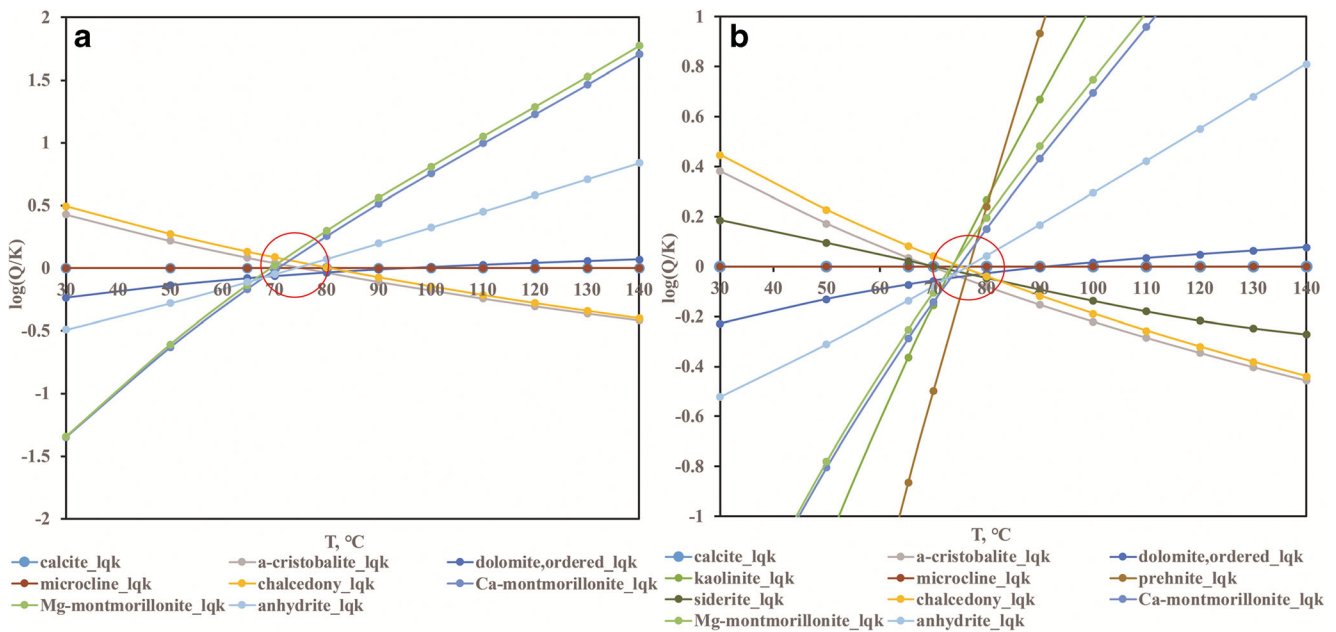


Fig. 9 Variation of mineral saturation indices (SI) with increasing temperature for samples **a** 16D05 and **b** 16D07. The convergence point indicates the calculated reservoir temperature

(LMWL, $\delta^2\text{H} = 8.3\delta^{18}\text{O} + 16.3\text{‰}$) was established with isotopic data from the Nanjing monitoring station of the Global Network of Isotopes in Precipitation (GNIP; IAEA/WMO 2017). The isotopic precipitation weighted average of the local meteoric water is $\delta^{18}\text{O} = -7.7\text{‰}$ and $\delta^2\text{H} = -49.2\text{‰}$. The CSW samples mainly originated from local precipitation according to field investigations. The CSW samples are enriched in ^2H and ^{18}O and lie in the lower right region of the LMWL (Fig. 3), indicating the evaporation effect (Clark and Fritz 1997). The local evaporation line (LEL) was established using a linear regression algorithm. The value of the intersection of LMWL and LEL is $\delta^{18}\text{O} = -7.8$ and $\delta^2\text{H} = -48.4\text{‰}$, which is very close to the isotopic precipitation weighted average of local meteoric water, suggesting the rationality of the established LMWL to some extent.

Although both the GG and CSG samples lie on or near the LMWL (Fig. 3), they are completely separated (except for 16D04) on Fig. 3 with isotopes in CSG samples being more enriched. This suggests that both GG and CSG were recharged by local precipitation, but the hydraulic connections between them are very limited. A remarkable oxygen isotope shift in Tangshan geothermal waters was not observed probably due to low reservoir temperature (Pang 2011), proving the reasonability of the aforementioned reservoir temperature calculation. The depleted isotopic composition in GG samples may be related to high recharge elevation.

The isotopic elevation effect of $\delta^{18}\text{O}$ can be used to evaluate groundwater recharge elevation (Clark and Fritz 1997):

$$h_R = \frac{\delta_G - \delta_P}{K} + h_G \quad (6)$$

where h_R is the recharge elevation, δ_G is the isotopic value of groundwater samples, δ_P is the isotopic value of local precipitation, h_G is the sampling point elevation of groundwater and K is the elevation gradient of $\delta^{18}\text{O}$. In this study, the isotopic precipitation weighted average of $\delta^{18}\text{O} = -7.7\text{‰}$ was assumed for δ_P , the average elevation gradient of the low latitude zone in southern China of $-0.3\text{‰}/100\text{ m}$ was assumed for K (Wang and Wang 2011). The calculation results of recharge elevation of GG are shown in Table 4. The recharge elevation varies from 137.5 to 301.9 m a.s.l., which is close to the elevation range of Tangshan. The calculation result of 16D04 is a negative value, which is probably due to significant mixing with CSG during upwelling.

Both the major hydrochemical compositions (Na, Ca, Mg, Sr, SO_4 , HCO_3 , Cl) and isotopic compositions ($\delta^2\text{H}$, $\delta^{18}\text{O}$, $\delta^{34}\text{S}$, $^{87}\text{Sr}/^{86}\text{Sr}$) are significantly different between GG and CSG, indicating weak hydraulic connections between them. Additionally, the permeability of the regionally distributed

Table 4 Calculation results of recharge elevation for geothermal groundwater (GG) samples

Sample ID	$\delta^{18}\text{O}$ (‰)	$\delta^2\text{H}$ (‰)	Recharge elevation (m a.s.l.)
16D01	-8.1	-52.9	137.5
16D02	-8.5	-55.7	282.2
16D03	-8.4	-55.8	246.9
16D04	-7.5	-49.1	-56.2
16D05	-8.3	-55.4	225.4
16D06	-8.2	-53.1	175.2
16D07	-8.6	-55.4	301.9

sandstone and shale of Silurian and Cretaceous systems overlying the geothermal reservoir in Tangshan is much lower (regarded as aquitards). It is hard for precipitation to penetrate through them to recharge the geothermal reservoir. On the other hand, the H and O stable isotopes suggest that the GG in Tangshan was recharged by local precipitation and the recharge elevation is close to the elevation range of Tangshan. Both the hydrochemical and isotopic compositions demonstrated that the GG in Tangshan mainly flowed through carbonate formation and reacted with carbonate minerals and anhydrite (gypsum). Furthermore, the body of Tangshan is distributed with exposed Cambrian and Ordovician carbonate rock with lots of NE and NW fault tectonics developed, which is conducive for receiving precipitation recharge to the geothermal reservoir. From the aforementioned text, the body of Tangshan distributed with exposed Cambrian and Ordovician carbonate rock is the most possible recharge zone for Tangshan GG. The precipitation penetrated through the carbonate formation of Cambrian and Ordovician systems to deeper layers and was heated up by the geothermal reservoir. The heated water then circulated upward along tectonic fissure to surface due to encountering the low permeability of sandstone and shale of the Silurian and Cretaceous strata overlying the geothermal reservoir, and mixed with cold shallow karstic water during upwelling.

Mixing model based on Sr and $^{87}\text{Sr}/^{86}\text{Sr}$

Mixing with shallow cold groundwater often occurs for geothermal water during upwelling (Guo et al. 2010, Guo et al. 2017). Both the hydrochemical compositions (Figs. 7b–d and 8) and isotopic compositions (Figs. 4 and 5) suggest the occurrence of mixing between GG and cold groundwater especially for sample 16D04. In order to validate the mixing process, a binary mixing model between two endmembers using Sr and $^{87}\text{Sr}/^{86}\text{Sr}$ (Bakari et al. 2013; Faure 1986; Négre et al. 2004) was considered:

$$\left(\frac{^{87}\text{Sr}}{^{86}\text{Sr}}\right)_m \times [\text{Sr}]_m = f \times \left(\left[\frac{^{87}\text{Sr}}{^{86}\text{Sr}}\right]_1 \times [\text{Sr}]_1 \right) + (1-f) \times \left(\left[\frac{^{87}\text{Sr}}{^{86}\text{Sr}}\right]_2 \times [\text{Sr}]_2 \right) \quad (7)$$

where $(^{87}\text{Sr}/^{86}\text{Sr})_m$ is the measured isotopic ratio, $[\text{Sr}]_m$ is the

measured Sr concentration in the mixture, $(^{87}\text{Sr}/^{86}\text{Sr})_1$ and $(^{87}\text{Sr}/^{86}\text{Sr})_2$ represent the isotopic ratios of the first and second endmembers, respectively, $[\text{Sr}]_1$ and $[\text{Sr}]_2$ the Sr concentrations of the two endmembers, respectively, and f is the fraction of endmember 1.

Since the hydraulic connections between deep GG in karstic aquifers and shallow groundwater in fractured aquifers of clastic rocks are weak, the mixing between deep GG and cold shallow karstic groundwater during upwelling is the most possible. The $^{87}\text{Sr}/^{86}\text{Sr}$ values of samples 16D08, 16D28 and 16D47 are below 0.710 and closest to that of GG among all the CSG samples, which therefore are considered as cold shallow karstic groundwater. These three samples lie approximately along a mixing line with GG samples (Fig. 4a); therefore, sample 16D28 ($^{87}\text{Sr}/^{86}\text{Sr} = 0.709563$, Sr = 846.0 $\mu\text{g/L}$), closest to GG samples (Fig. 4a), was assumed for the cold water endmember. The three samples of 16D03/16D05/16D07 with the highest wellhead temperature have similar lowest $^{87}\text{Sr}/^{86}\text{Sr}$ and highest Sr content. Here the average ($^{87}\text{Sr}/^{86}\text{Sr} = 0.709170$, Sr = 9914.0 $\mu\text{g/L}$) of the three samples was assumed for the value of the geothermal water endmember. The calculation results are shown in Table 5. Sample 16D04 has the highest mixing fraction (63.1%) of cold water proving the speculation previously discussed, deduced from hydrochemical and isotopic results. Other samples have the low mixing fraction (around 30%) of cold water.

^{14}C age of geothermal water

This study used ^{14}C to evaluate the age of GG in Tangshan. The ^{14}C age (t) of groundwater was determined by the following equation:

$$t = -8267 \times \ln \frac{a_t}{a_0} \quad (8)$$

where a_t is the measured ^{14}C content in groundwater samples, and a_0 is the initial ^{14}C content. However, the dissolution of carbonate minerals can dilute the true initial ^{14}C activity of DIC in groundwater. The relationship between ^{14}C and $\delta^{13}\text{C}$ of GG samples is shown in Fig. 6. The ^{14}C value shows a decreasing trend with increasing $\delta^{13}\text{C}$, indicating the dilution effect of carbonate minerals dissolution. There are many models that can be used to correct the dilution effect. In this study, Tamers (1975), Fontes and Garnier (1979), Evans et al. (1979), Eichinger (1981), Pearson model (Pearson 1965) and

Table 5 Calculation results of the mixing fraction of geothermal groundwater (GG) samples

Sample ID	$^{87}\text{Sr}/^{86}\text{Sr}$	Sr ($\mu\text{g/L}$)	Thermal water fraction	Cold water fraction
16D01	0.709136	6921	0.670	0.330
16D02	0.709168	7466	0.730	0.270
16D04	0.709208	4191	0.369	0.631
16D06	0.709210	7304	0.712	0.288

Pearson model considering the isotopic fractionation between soil CO₂ and DIC (abbreviated as Pearson model No. 2; Clark and Frintz 1997) were adopted to correct the ¹⁴C age. The initial ¹⁴C activity of 100 pmC, δ¹³C of carbonate minerals of 0 ‰ and δ¹³C of soil CO₂ of −23 ‰ were assumed during the correction.

The age evaluation results are shown in Table 6. The results of Tamers, Fontes and Garnier, Evans, Eichinger and Pearson models include some negative age values which are not reasonable. Only the Pearson model No. 2 gives the relatively reasonable results which are considered as the corrected ¹⁴C age of GG in Tangshan. Although the corrected absolute age may deviate from the real age to some extent, it is believed to be more accurate than the uncorrected age and can indicate the age level of groundwater (Huang and Pang 2011). The age of GG in the east of Tangshan is relatively old (944–9,155 years) compared to that in the west of Tangshan (16D06 = 1,777 years). The lowest age of sample 16D04 probably resulted from mixing with shallow groundwater as previously discussed. In summary, the age of GG in Tangshan is on the level of millennial scale, which is consistent with the fact that GG samples are tritium-free.

Implications for sustainable use of geothermal water

Groundwater renewability refers to the ability to replace the groundwater extracted from the aquifer through recharge, naturally or artificially (Wang et al. 2011; Huang et al. 2017b). When geothermal reinjection is not implemented, renewability of geothermal water is judged in a similar way as to normal groundwater. The characteristics of groundwater age can reveal the groundwater circulation rate and renewability (Huang et al. 2017b). The age of GG in Tangshan is thousands of years, indicating very low circulation rate and rare renewability (Huang et al. 2017b). The GG in Tangshan was mainly recharged by local precipitation and the area of the recharge zone (Tangshan Mountain) is much limited (about 7 km²), rather than a large catchment basin, as in other cases. Due to these characteristics, overexploitation would likely lead to

depletion of geothermal water. Actually, rapid decline of the water table in Tangshan is already occurring, where all hot springs have vanished from the surface and some geothermal wells are being depleted, resulting from apparent overexploitation of the geothermal water. Continuous decline of the water table may accelerate the thermal breakthrough (cold-water recharge to the geothermal reservoir) which is detrimental for maintaining the reservoir temperature as stable (Axelsson 2010; Kong et al. 2014). To prevent the water table from further declining and to ensure the sustainable use of geothermal resources in Tangshan, continuous monitoring of the water table and a rational plan of utilization should be implemented. Used geothermal-water treatment and reinjection (Duan et al. 2011; Liu and Wang 2006) should be considered if possible, to maintain the geothermal water yield and reservoir pressure. In addition, to prevent the geothermal water from being contaminated and to ensure good water quality, the recharge zone (Tangshan Mountain) should be protected from being polluted.

Conclusions

A multi-tracer approach involving chemicals and isotopes (δ²H, δ¹⁸O, δ³⁴S, ⁸⁷Sr/⁸⁶Sr, δ¹³C, ¹⁴C, ³H) was conducted to provide insight into the recharge source and groundwater circulation in TGS. The application of chemical geothermometers, including cation ratios and Silica solubility, as well as thermodynamic modeling, revealed reservoir temperatures of 51 °C in the western side and 74–87 °C in the eastern side of Tangshan Mountain, respectively, which needs a groundwater circulation depth of about 2.5 km. The geothermal water in TGS was recharged by past (1,777–9,155 years) local precipitation with depleted δ²H and δ¹⁸O, through the Cambrian and Ordovician carbonate formations area exposed on the upper part of the mountain. The parent geothermal water was cooled due to mixing with shallow cold karstic groundwater during upwelling with a cold-water mixing fraction up to 63%. The corrected ¹⁴C age of geothermal water is

Table 6 Calculation results of ¹⁴C age of the geothermal groundwater (GG) samples based on different models (in years)

Sample ID	δ ¹³ C (‰)	¹⁴ C (pmC)	Uncorrected	Tamers model	Pearson model	Fontes and Garnier model	Evans model	Eichinger model	Pearson model No. 2
16D01	−10.1	50.2	5,697	961	−759	−948	−1,778	2,989	2,151
16D02	−13.2	30.8	9,735	4,164	−1	−1	−1	13,871	9,155
16D03	−7.3	21.4	12,745	7,920	3,835	3,173	1,637	9,906	6,580
16D04	−12.5	76.9	2,171	−3,220	−2,639	−2,414	−3,048	−1,272	944
16D05	−8.0	26.1	11,104	6,021	2,879	2,402	965	8,522	5,880
16D06	−11.4	59.9	4,237	−595	−1,288	−1,330	−1,765	713	1,777
16D07	−9.1	30.6	9,789	4,412	2,538	2,276	979	7,525	5,915

on the millennial scale, indicating a low circulation rate and rare renewability. The recovery of the water table occasionally occurring in some production wells may be attributed to the effect of pressure migration but not the present-day rainfall recharge.

This study provided key information on the water origin of TGS and the results are instructive and significant with respect to the sustainable exploitation of geothermal resources in Tangshan. It is recommended that a monitoring network of wells be established that would include regular measurements of the groundwater level, down-hole temperature and chemistry. Prediction of future changes in the flow and geotemperature field would become possible if integrated with numerical reservoir modeling. Reinjection of used geothermal water is another possibility to be considered that would help maintain the pressure of the system. The methodology tested here can also be applied to evaluate other geothermal systems.

Acknowledgements Thanks are due to Prof. Huang Jinsheng and Prof. Luo Zhujiang for their discussions during the project implementation. Appreciation goes to Prof. Jin Zhengang and Prof. Li Yiman, who helped with stable isotope and hydrochemical analyses, respectively. The authors are also grateful to the two anonymous reviewers and guest editor Prof. Dr. Wenke Wang whose insightful comments were very helpful in improving the quality of the manuscript.

Funding Information The reported study is partly financially supported by the National Natural Science Foundation of China (NSFC Grant 41430319), the 1st Geological Brigade of Jiangsu Geology and Mineral Exploration Bureau and the UCAS (UCAS [2015]37) Joint PhD Training Program.

References

- Al-Charideh A (2015) Isotopic evidence to characterize the sources of sulfate ions in the carbonate aquifer system in Aleppo basin (North Syria). *Environ Earth Sci* 73(1):127–137
- Amorsson S, Gunnlaugsson E, Svavarsson H (1983) The chemistry of geothermal waters in Iceland: III. chemical geothermometry in geothermal investigations. *Geochim Cosmochim Acta* 47(3):567–577
- Awaleh MO, Hoch FB, Boschetti T, Soubaneh YD, Egueh NM, Elmi SA, Mohamed J, Khairah MA (2015) The geothermal resources of the Republic of Djibouti, II: geochemical study of the Lake Abhe geothermal field. *J Geochem Explor* 159: 129–147
- Axelsson G (2010) Sustainable geothermal utilization-case histories, definitions, research issues and modelling. *Geothermics* 39(4):283–291. <https://doi.org/10.1016/j.geothermics.2010.08.001>
- Bakari SS, Aagaard P, Vogt RD, Ruden F, Johansen I, Vuai SA (2013) Strontium isotopes as tracers for quantifying mixing of groundwater in the alluvial plain of a coastal watershed, south-eastern Tanzania. *J Geochem Explor* 130:1–14
- Barbieri M, Morotti M (2003) Hydrogeochemistry and strontium isotopes of spring and mineral waters from Monte Vulture volcano, Italy. *Appl Geochem* 18:117–125
- Bo Y, Liu C, Zhao Y, Wang L (2015) Chemical and isotopic characteristics and origin of spring waters in the Lanping–Simao Basin, Yunnan, southwestern China. *Chem Erde-Geochem* 75(3):287–300
- Boschetti T, Venturelli G, Toscani L, Barbieri M, Mucchino C (2005) The Bagni di Lucca thermal waters (Tuscany, Italy): an example of Ca-SO₄ waters with high Na/Cl and low Ca/SO₄ ratios. *J Hydrol* 307: 270–293
- Bozdağ A (2016) Hydrogeochemical and isotopic characteristics of Kavak (Seydişehir-Konya) geothermal field, Turkey. *J Afr Earth Sci* 121:72–83
- Brenot A, Négrel P, Petelet-Giraud E, Millot R, Malcuit E (2015) Insights from the salinity origins and interconnections of aquifers in a regional scale sedimentary aquifer system (Adour-Garonne district, SW France): contributions of $\delta^{34}\text{S}$ and $\delta^{18}\text{O}$ from dissolved sulfates and the $^{87}\text{Sr}/^{86}\text{Sr}$ ratio. *Appl Geochem* 53:27–41
- Chandrajith R, Barth JAC, Subasinghe ND, Merten D, Dissanayake CB (2013) Geochemical and isotope characterization of geothermal spring waters in Sri Lanka: evidence for steeper than expected geothermal gradients. *J Hydrol* 476:360–369
- Clark ID, Fritz P (1997) Environmental isotopes in hydrogeology. CRC, Boca Raton, FL, 328 pp
- Diamond RE, Harris C (2000) Oxygen and hydrogen isotope geochemistry of thermal springs of the Western Cape, South Africa: recharge at high altitude? *J Afr Earth Sci* 31(3/4):467–481
- Duan Z, Pang Z, Wang X (2011) Sustainable evaluation of limestone geothermal reservoirs with extended production histories in Beijing and Tianjin, China. *Geothermics* 40:125–135. <https://doi.org/10.1016/j.geothermics.2011.02.001>
- Edmunds WM, Ma J, Aeschbach-Hertig W, Kipfer R, Darbyshire DPF (2006) Groundwater recharge history and hydrogeochemical evolution in the Minqin Basin, North West China. *Appl Geochem* 21(12): 2148–2170
- Eichinger L (1981) Age determination of groundwaters by means of carbon-14: measurement and interpretation of groundwaters of the Frankonian Albvorland. PhD Thesis, University of Munich, Germany
- Evans GV, Otlet RL, Downing A, Monkhouse RA, Rae G (1979) Some problems in the interpretation of isotope measurements in United Kingdom aquifer. *Isotope Hydrol* 2:639–708
- Faure G (1986) Principles of isotope geology. Wiley, Chichester, UK
- Fontes J-C, Garnier JM (1979) Determination of initial ^{14}C activity of the total dissolved C: a review of the existing models and a new approach. *Water Resour Res* 15:399–413
- Fournier RO (1977) Chemical geothermometers and mixing models for geothermal systems. *Geothermics* 5:41–50
- Fournier RO (1979) A revised equation for Na/K geothermometers. *Geoth Res Counc Trans* 3:221–224
- Fournier RO (1991) Water geothermometers applied to geothermal energy. In: D'Amore F (ed) Applications of geochemistry in geothermal reservoir development. UNITAR/UNDP, Rome, pp 37–69
- Fournier RO, Potter RW (1979) Magnesium correction to the Na-K-Ca chemical geothermometer. *Geochim Cosmochim Acta* 43:1543–1550
- Fournier RO, Truesdell AH (1973) An empirical Na-K-Ca geothermometer for natural waters. *Geochim Cosmochim Acta* 37: 1255–1275
- Ghomshei MM, Clark ID (1993) Oxygen and hydrogen isotopes in deep thermal waters from the South Meager Creek geothermal area, British Columbia, Canada. *Geothermics* 22(2):79–89
- Giggenbach WF (1988) Geothermal solute equilibria-derivation of Na-K-Mg-Ca geothermometers. *Geochim Cosmochim Acta* 52:2749–2776
- Grobe M, Machel HG, Heuser H (2000) Origin and evolution of saline groundwater in the Munsterland cretaceous basin, Germany: oxygen, hydrogen, and strontium isotope evidence. *J Geochem Explor* 69:70:5–9
- Guo Q, Wang Y, Liu W (2010) O, H, and Sr isotope evidences of mixing processes in two geothermal fluid reservoirs at Yangbajing, Tibet, China. *Environ Earth Sci* 59(7):1589–1597

- Guo Q, Pang Z, Wang Y, Tian J (2017) Fluid geochemistry and geothermometry applications of the Kangding high-temperature geothermal system in eastern Himalayas. *Appl Geochem*. <https://doi.org/10.1016/j.apgeochem.2017.03.007>
- Hähnlein S, Bayer P, Ferguson G, Blum P (2013) Sustainability and policy for the thermal use of shallow geothermal energy. *Energy Pol* 59:914–925
- Han L, Plummer LN, Aggarwal P (2014) The curved ^{14}C vs. $\delta^{13}\text{C}$ relationship in dissolved inorganic carbon: a useful tool for groundwater age- and geochemical interpretations. *Chem Geol* 387:111–125
- Huang T, Pang Z (2011) A combined conceptual model (V&P model) to correct groundwater radiocarbon age. In: *Proceedings of 2011 International Symposium on Water Resource and Environmental Protection*, vol 1 (ISWREP). IEEE, Piscataway, NJ
- Huang T, Pang Z, Liu J, Ma J, Gates J (2017a) Groundwater recharge mechanism in an integrated tableland of the Loess Plateau, northern China: insights from environmental tracers. *Hydrogeol J*. <https://doi.org/10.1007/s10040-017-1599-8>
- Huang T, Pang Z, Li J, Xiang Y, Zhao Z (2017b) Mapping groundwater renewability using age data in the Baiyang alluvial fan, NW China. *Hydrogeol J* 25(3):743–755
- IAEA/WMO (2017) The GNIP database. Available at <http://www.iaea.org/water>. Accessed January 2018
- Khask M, La Salle CLG, Videau G, Flinois JS, Frappe S, Team A, Verdoux P (2015) Deep water circulation at the northern Pyrenean thrust: implication of high temperature water–rock interaction process on the mineralization of major spring water in an overthrust area. *Chem Geol* 419:114–131
- Kong Y, Pang Z, Shao H, Hu S, Kolditz O (2014) Recent studies on hydrothermal systems in China: a review. *Geotherm Energy* 2:19
- Kong Y, Pang Z, Pang J, Luo L, Luo J, Shao H, Kolditz O (2015) Deep groundwater cycle in Xiongxin geothermal field. *Proceedings World Geothermal Congress 2015*, Melbourne, Australia, April 19–25, 2015
- Li A, Zhu C, Yang S (2010) The research on formation condition of Tangshan Warm Spring in Nanjing (in Chinese with English abstract). *Mineral Explor* 1(6):546–549
- Li G, Li F (2010) The circulation law, sustainable development and utilization of geothermal water in Guanzhong Basin. Science Press, Beijing, 100 pp
- Li Y, Pang Z, Yang F, Yuan L, Tang P (2017) Hydrogeochemical characteristics and genesis of the high-temperature geothermal system in the Tashkorgan basin of the Pamir Syntax, western China. *J Asian Earth Sci* 149:134–144
- Liu J, Wang K (2006) Geothermal reinjection in China. *Proceedings of the 7th Asian Geothermal Symposium*, July 25–26, 2006
- Luan G, Qiu H (1998) The type of low-medium temperature geothermal system of convection type: the genesis analysis of Tangshan geothermal system in Nanjing (in Chinese with English abstract). *J Ocean Univ Qingdao* 28(1):156–160
- Lund JW, Boyd TL (2016) Direct utilization of geothermal energy 2015 worldwide review. *Geothermics* 60:66–93
- Ma T, Wang Y, Guo Q, Yan C, Ma R, Huang Z (2009) Hydrochemical and isotopic evidence of origin of thermal karst water at Taiyuan, northern China. *J Earth Sci* 20(5):879–889
- Ma R, Wang Y, Sun Z, Zheng C, Ma T, Prommer H (2011) Geochemical evolution of groundwater in carbonate aquifers in Taiyuan, northern China. *Appl Geochem* 26(5):884–897
- Majumdar N, Majumdar RK, Mukherjee AL, Bhattacharya SK, Jani RA (2005) Seasonal variations in the isotopes of oxygen and hydrogen in geothermal waters from Bakreswar and Tantloi, eastern India: implications for groundwater characterization. *J Asian Earth Sci* 25:269–278
- Michael K, Golab A, Shulakova V, Ennis-King J, Allinson G, Sharma S, Aiken T (2010) Geological storage of CO_2 in saline aquifers: a review of the experience from existing storage operations. *Int J Greenh Gas Con* 5:659–667
- Mongillo MA (2010) Preface to geothermics special issue on sustainable geothermal utilization. *Geothermics* 39:279–282
- Montanari D, Minissale A, Doveri M, Gola G, Trumphy E, Santilano A, Manzella A (2017) Geothermal resources within carbonate reservoirs in western Sicily (Italy): a review. *Earth-Sci Rev* 169:180–201
- Négrel P, Roy S (1998) Chemistry of rainwater in the Massif Central (France): a strontium isotope and major element study. *Appl Geochem* 13(8):941–952
- Négrel P, Petelet-Giraud E, Widory D (2004) Strontium isotope geochemistry of alluvial groundwater: a tracer for groundwater resources characterization. *Hydrol Earth Syst Sci* 8(5):959–972
- Pang Z (2011) Geothermal waters. In: Gu W, Pang Z, Wang J, Song X (eds) *Isotope hydrology* (in Chinese with English abstract). Science Press, Beijing, pp 576–588
- Pang Z, Reed M (1998) Theoretical chemical thermometry on geothermal waters: problems and methods. *Geochim Cosmochim Acta* 62:1083–1091
- Pang Z, Yang F, Luo L (2013) Approaches in determining geothermal reservoir temperatures: a review. In: Ding Z (ed) *Methodologies in solid earth sciences* (in Chinese). Science Press, Beijing, pp 219–242
- Pang Z, Pang J, Kong Y, Luo L, Duan Z, Yang F, Wang S (2015) Large karstic geothermal reservoirs in sedimentary basins in China: genesis, energy potential and optimal exploitation. *Proceedings of World Geothermal Congress 2015*, Melbourne, Australia, April 19–25, 2015
- Parkhurst DL, Appelo CAJ (2013) Description of input and examples for PHREEQC Version 3: a computer program for speciation, batch-reaction, one-dimensional transport, and inverse geochemical calculations. *US Geol Surv Tech Methods* 6-A43. Available at <http://pubs.usgs.gov/tm/06/a43/>. Accessed January 2017
- Pearson FJ (1965) Use of $^{13}\text{C}/^{12}\text{C}$ ratios to correct radiocarbon ages of material initially diluted by limestone. In: *Proceedings of the 6th International Conference on Radiocarbon and Tritium Dating*, Pullman, WA, June 1965, 357 pp
- Raidla V, Kirsimäe K, Ivask J, Kaup E, Knöller K, Marandi A, Martma T, Vaikmäe R (2014) Sulphur isotope composition of dissolved sulphate in the Cambrian-Vendian aquifer system in the northern part of the Baltic Artesian Basin. *Chem Geol* 383:147–154
- Reed M, Spycher N (1984) Calculation of pH and mineral equilibria in hydrothermal waters with application to geothermometry and studies of boiling and dilution. *Geochim Cosmochim Acta* 48:1479–1492
- Reinsch T, Hennings J, Asmundsson R (2013) Thermal, mechanical and chemical influences on the performance of optical fibres for distributed temperature sensing in a hot geothermal well. *Environ Earth Sci* 70:3465–3480. <https://doi.org/10.1007/s12665-013-2248-8>
- Sack AL, Sharma S (2014) A multi-isotope approach for understanding sources of water, carbon and sulfur in natural springs of the central Appalachian region. *Environ Earth Sci* 71(11):4715–4724
- Spycher N, Peiffer L, Sonnenthal, E (2013) *GeoT user's guide a computer program for multicomponent geothermometry and geochemical speciation version 1.4*. Report no. LBNL-6172E, Lawrence Berkeley National Laboratory, Berkeley, CA
- Tamers MA (1975) Validity of radiocarbon dates of groundwater. *Geol Surv* 2:217–239
- Tonani F (1980) Some remarks on the application of geochemical techniques in geothermal exploration. In: Strub AS, Ungemach P (eds) *Advances in European geothermal research*. Springer, Dordrecht, The Netherlands, pp 428–443
- Truesdell AH (1976) Summary of section III: geochemical techniques in exploration. In: *Proc. of the 2nd United Nations Symp. on the Development and Use of Geothermal Resources*, San Francisco, May 1975, pp 53–79

- Wang D, Wang K (2011) Hydrogen and oxygen isotope characteristics of precipitation. In: Gu W, Pang Z, Wang J, Song X (eds) *Isotope hydrology* (in Chinese with an English abstract). Science Press, Beijing, pp 150–173
- Wang G, Li K, Wen D, Lin W, Lin L, Liu Z, Zhang W, Ma F, Wang W (2015) Assessment of geothermal resources in China. In: *Proceedings of the World Geothermal Congress 2015*, Melbourne, Australia
- Wang J (2009) Discussions on geothermal energy exploration and utilization of China, from the point of world geothermal energy. *Proceedings of workshop on Chinese scientific geothermal energy exploration*. Geology Press, Beijing, pp 3–6
- Wang J, Xiong L, Pang Z (1993) Low-middle convective geothermal system (in Chinese). Science Press, Beijing
- Wang J, Zhai Y, Teng Y, Zuo R (2011) Study on groundwater renewal capacity and reproducibility (in Chinese). *J Beijing Normal Univ Nat Sci* 42:213–216
- Wang P, Chen X, Shen L, Wu K, Huang M, Xiao Q (2016) Geochemical features of the geothermal fluids from the Mapamyum non-volcanic geothermal system (western Tibet, China). *J Volcanol Geoth Res* 320:29–39
- Wang Y, Guo Q, Su C, Ma T (2006) Strontium isotope characterization and major ion geochemistry of karst water flow, Shentou, northern China. *J Hydrol* 328(3):592–603
- Xu W, Su X, Dai Z, Yang F, Zhu P, Huang Y (2017) Multi-tracer investigation of river and groundwater interactions: a case study in Nalenggele River basin, northwest China. *Hydrogeol J* 25(7):2015–2029. <https://doi.org/10.1007/s10040-017-1606-0>
- Yang P, Cheng Q, Xie S, Wang J, Chang L, Yu Q, Zhan Z, Chen F (2017) Hydrogeochemistry and geothermometry of deep thermal water in the carbonate formation in the main urban area of Chongqing, China. *J Hydrol* 549:50–61
- Zhao J, Zhu S (1998) Control factors and resources Prospect of geothermal water in Tangshan Hill of Nanjing, Jiangsu (in Chinese with English abstract). *Geology* 22(4):242–248
- Zou P, Qiu Y, Wang C (2015) Analyses of the genesis of Tangshan Hot Spring area in Nanjing (in Chinese with English abstract). *Geol J China Univ* 21(1):155–162